

WAVE BREAKING FUNCTION

Lihwa Lin¹ and Ray-Qing Lin²

¹ U.S. Army Engineer Research and Development Center
3909 Halls Ferry Road, Vicksburg, MS. 39180

² David Taylor Model Basin, Division of Seakeeping,
9500 MacArthur Blvd, West Bethesda, NSWCCD, MD 20817-5700

1. INTRODUCTION

Wave breaking is a major sink mechanism for the water surface gravity waves. In 1893, Michell first suggested that the monochromatic wave has a limiting steepness, $(ak)_{\max} = 0.44$, where a is the wave amplitude and k is the wave number. In 1977 and 1978, Longuet-Higgins and Fox developed a simple wave-breaking model that is still used by today's wave prediction communities. More recently, an advanced WAM model (WAMDI group, 1988) calculates the spectral wave breaking based on the state-of-the-art formulation. However, the wave-breaking phenomenon at sea is still far from being fully understood. In the present study, a new wave-breaking formula at the ocean model scale was investigated based on physical processes observed in intermediate depth water.

Existing wave-breaking formulas generally include basic wave parameters computed in WAM, such as the mean wave steepness, \bar{s} , where $s = ak$, mean phase velocity, \bar{c} , and energy density, $E(\sigma, \theta)$ in the frequency σ and direction θ domain. However, using these formulas can sometimes be misleading because wave breaking is likely more affected by individual wave characteristics rather than mean wave properties. The proper formula shall also include wind speed, \bar{u}_{wind} and wind direction, θ_{wind} , because the wind can modify the water particle velocity under the wave motion. When the wind direction is the same as the wave propagation direction, the wind stress tends to increase the water particle velocity and, at the same time, create a surface current in the down wind direction. Under this condition, waves become less vulnerable to overturning and, therefore, experience weaker breaking. When wind and wave directions are opposite to each other, the wind and wind-driven surface current can reduce the water particle velocity under the wave motion to cause stronger wave breaking in the high frequency range. Phillips and Banner (1974), by investigating the surface turbulent flow in laboratory experiments, suggested the wind speed indeed does impact the wave breaking. In the new wave breaking formula, both wave steepness, s , and phase velocity, \bar{c}_{σ} , are calculated for individual wave frequency components because they vary with the frequency. The increased breaking of short waves riding on long waves and the factor of water depth, h , are also included in the new formula.

To illustrate the new wave-breaking formula, a series of directional spectra measured in the offshore of Cape Fear, NC, available from 2000 to 2003 were selected for the following two cases: (1) light wind, with steady magnitude and direction, blowing in the same direction as the average wave propagation, and (2) mild wind, with steady magnitude and direction, blowing in the opposite direction of the average wave propagation.

2. FIELD DATA

Ocean waves usually appear in irregular forms and propagate in multiple directions. To study the physical phenomena of ocean waves, it is meaningful to use data collected in the field. In the present study, wind and wave measurements in the offshore of Cape Fear, NC, were selected for the investigation of wave breaking function. Wave data were collected as time series of directional wave energy spectra from five wave gauges maintained by the Wilmington Harbor Monitoring Program (<http://www.frf.usace.army.mil/capefear>). The wave data collection was conducted in a three-year period

from September 2000 to June 2003. Figure 1 shows the location of the five wave gauges relative to Cape Fear. Table 1 presents the location, water depth, and data collection time periods of the five wave gauges. Offshore sea surface wind data are available from two meteorological stations maintained by the National Data Buoy Center (<http://www.ndbc.noaa.gov>). Figure 2 shows the location map of the two meteorological stations and Table 2 presents the location, water depth, and data collection period of the two stations. It is noted that the two meteorological stations also measured wave energy spectra in 2000-2003. However, because these wave spectra measured from the two meteorological stations do not contain the wave direction information, they were not used in the wave breaking function investigation.

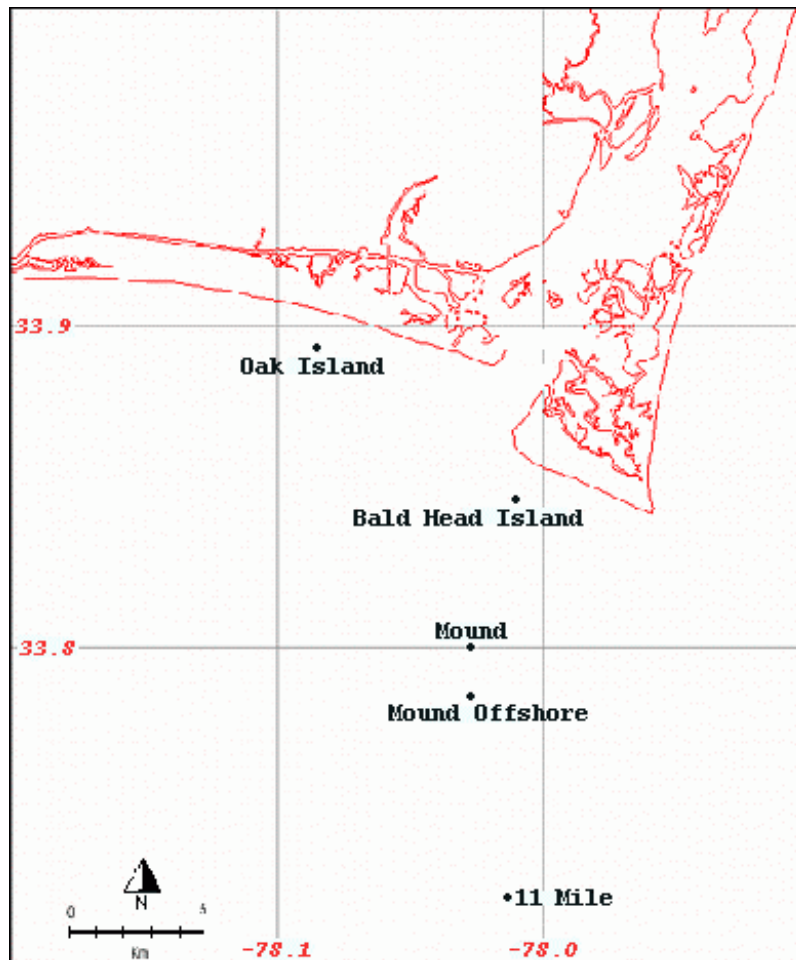


Figure 1. Location map of directional wave gauges

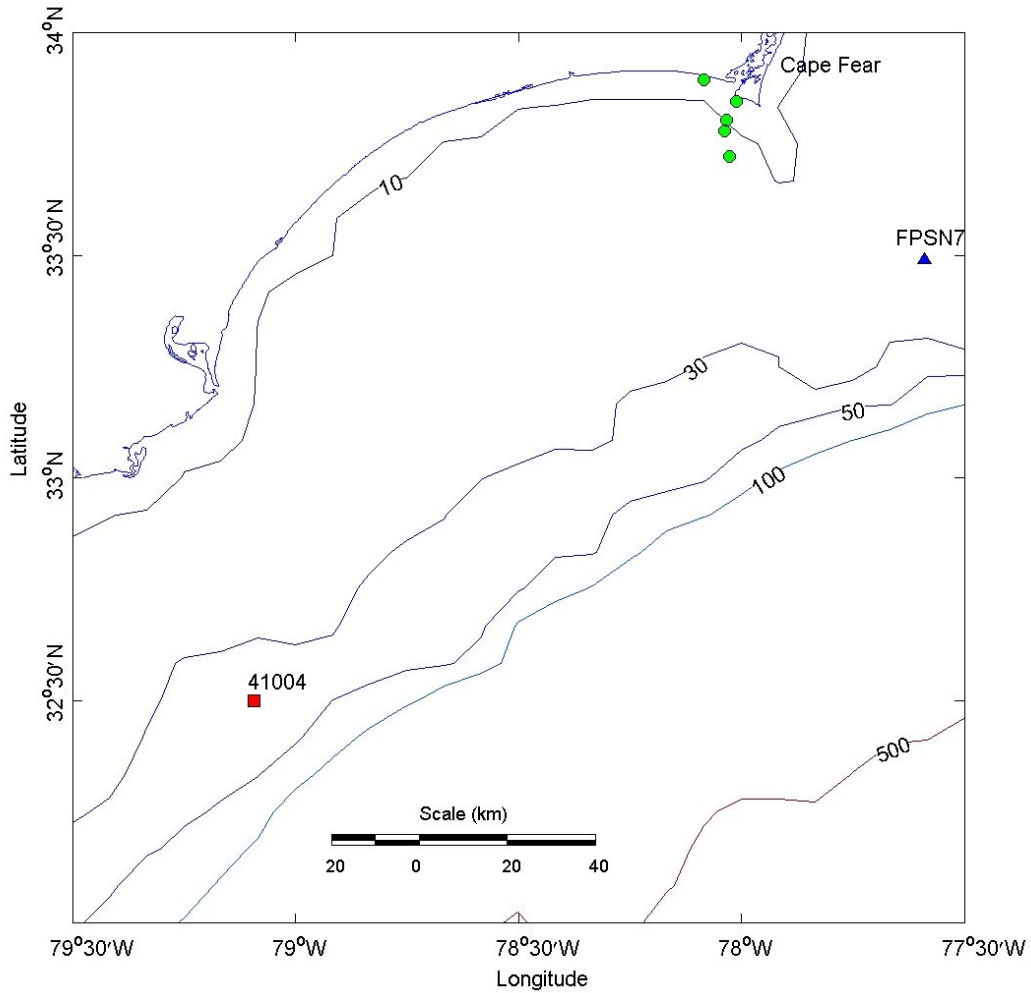


Figure 2. Location of meteorological stations (depth contours in meters)

Table 1 Directional Wave Gauge Information			
Station	Coordinates	Nominal depth (m)	Data collection period
Oak Island	33° 53' 40" N, 78° 05' 04" W	7	September 2000 – May 2003
Bald Head Island	33° 53' 02" N, 78° 00' 40" W	5.8	September 2000 – June 2003
Mound Crest	33° 48' 13" N, 78° 02' 02" W	7	July 2001 – June 2002
Mound Offshore	33° 46' 48" N, 78° 02' 15" W	12.8	August 2001 – July 2002
Mile 11	33° 43' 17" N, 78° 01' 32" W	12.8	September 2000 – June 2003

Table 2 Meteorological Station Information			
Station	Coordinates	Nominal depth (m)	Data collection period
FPSN7	33° 29' 24" N, 77° 35' 24" W	14	November 1984 – present
Buoy 41004	32° 30' 36" N, 79° 06' 00" W	38	June 1978 – present

3. WAVE BREAKING FUNCTION

3.1 Previous Models

By neglecting the viscous effect of the seawater, the wave energy dissipation can be divided into three categories: (1) white-capping, $S_{wc}(\sigma, \theta)$; (2) bottom friction, $S_b(\sigma, \theta)$; and (3) depth-limited breaking, $S_{br}(\sigma, \theta)$.

(1) White-capping in WAM is based on the wave steepness (Michell, 1893; Hasselmann, 1974; Komen et al. 1994):

$$S_{wc}(\sigma, \theta) = C_{ds} \bar{S}^n \frac{\bar{\sigma}}{k} kE(\sigma, \theta), \quad (1)$$

where $\bar{\sigma}$, \bar{k} , and \bar{S} denote the mean frequency, mean wave number, and overall mean wave steepness, respectively. Here, C_{ds} and n are empirically estimated coefficients ($C_{ds} = 2.36 \times 10^{-5}$, and $n=4$). If a swell is present at the same time with wind waves such that \bar{S} is decreasing, and the mean phase velocity $\bar{c} = \frac{\bar{\sigma}}{\bar{k}}$ is increasing, then the overall white-capping will be decreasing. This contrasts to the observational data presented by Donelan in 1987 (Holthuijsen and Booij, 2000).

(2) Bottom friction (Hasselmann et al. 1973):

$$S_b(\sigma, \theta) = -C_b \frac{\sigma^2}{g^2 \sinh^2(kh)} E(\sigma, \theta), \quad (2)$$

where C_b is a proportional constant.

(3) Depth-limited breaking (Eldeberky and Battjes, 1995; Holthuijsen and Booij, 2000):

$$S_{br} = -\frac{D_{tot}}{E_{tot}} E(\sigma, \theta), \quad (3)$$

where D_{tot} is a function of a_{wave}/h and a_{wave} , where a_{wave} is the amplitude of water surface waves, and E_{tot} is the total wave energy. Equation (3) generally shows good agreement with the observed data (Holthuijsen and Booij, 2000). However, if $2a_{wave}/h=0.73$ and is treated as a constant, applying Equation (3) for wave breaking will not to be universal.

3.2 Wave Breaking Function in a New Coastal Wave Model (Lin and Huang, 1976a and b, Lin and Perrie, 1997a and b, 1999):

The bottom friction function expressed in Equation (2) is applied in WAM (Hasselmann et al. 1973) and is more effective in the shallow water region. The present study will focus only on the wave breaking as a result of white-capping and depth-dependent breaking effects in intermediate depth water.

Observed Wave Breaking in the Intermediate Water

To investigate the wave breaking function using the observed data, it is convenient to select the case with small or mild wind condition so that the wind input interference will be minimal. As a first example, Figure 3 shows two consecutive directional spectra (in the units of $m^2 \text{sec/radian}$) measured from Mile 11 at 05:35 and 08:35 GMT in November 29th, 2001 under a light wind condition (wind speed is 3m/sec, from 140°). In this example, the wind direction is similar to the mean wave direction from the SE. For the

spectrum measured at 05:35 GMT, the maximum energy density is $0.15 \text{ m}^2\text{sec/radian}$ and the associated propagation direction is 150° . For the spectrum measured at 08:35 GMT, the maximum energy density is $0.11 \text{ m}^2\text{sec/radian}$ and the associated propagation direction is 155° , also similar to the wind direction (140°). In both spectra, the peak energy density occurred at 0.095 Hz . These two spectra present a swell propagated from the open ocean or from the SE direction. The decrease of the maximum energy density is about $0.04 \text{ m}^2\text{sec/radian}$ or 26.7% in the interval of three hours.

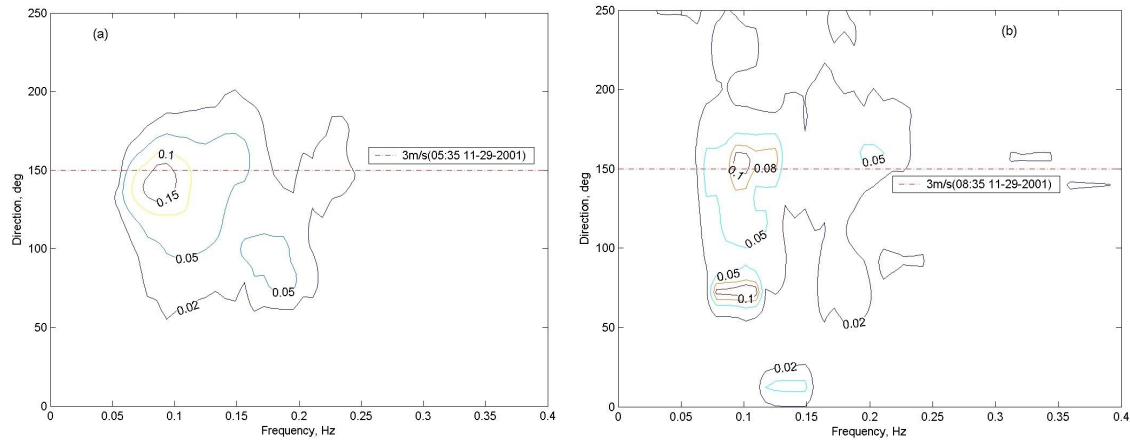


Figure 3. Measured directional wave spectra from Mile 11 at (a) 05:35 GMT and (b) 08:35 in November 29th, 2001 (surface wind is 3m/sec from 150° , shown as dash lines)

As a second example, Figure 4 shows two consecutive directional spectra from Mile 11 at 14:35 GMT and 17:35 GMT in November 7th, 2001, under a mild wind condition (wind speed is 6 m/sec from 280° at 14:35 GMT, and 7 m/sec from 265° at 17:35 GMT). In this example, the wind direction is somewhat opposite to a swell from the ocean (from the SSE direction). For the spectrum measured at 14:35 GMT, the maximum energy density of the swell is $0.10 \text{ m}^2\text{sec/radian}$ and the associated propagation direction is 160° . For the spectrum measured at 17:35 GMT, the maximum energy density is $0.06 \text{ m}^2\text{sec/radian}$ from the direction of 170° . In both spectra, the peak energy density of the swell occurred at 0.095 Hz . The decrease of the maximum energy density of the swell, as propagating against the wind, is about $0.04 \text{ m}^2\text{sec/radian}$ or 40% in the interval of three hours.

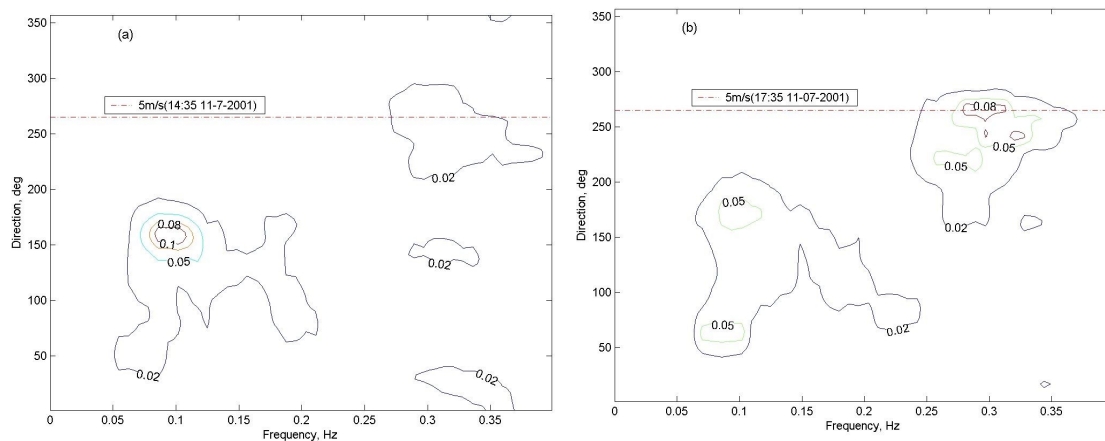


Figure 4. Measured directional wave spectra from Mile 11 at (a) 14:35 GMT and (b) 17:35 GMT in November 7th, 2001 (surface wind is 5m/sec from 265° , as shown dash lines)

As a third example, Figure 5 shows two directional wave spectra measured from Mound Offshore and Oak Island at 13:00 GMT and 14:03 GMT in November 7th, 2001. These two spectra and the one in Figure 4a show the energy dissipation in the swell from the offshore (Mile 11) to the nearshore (Oak Island) locations. The energy loss in the swell from Mile 11 to Oak Island is more affected by the combined white-capping, depth limitation, and bottom friction effects. Note that the swell direction at the Oak Island station is more toward the shore normal (180°) as a result of wave refraction. The transformation of the swell spectrum from Mile 11 to Oak Island is also affected by wave shoaling as the swell propagated from the ocean to the shallow water location.

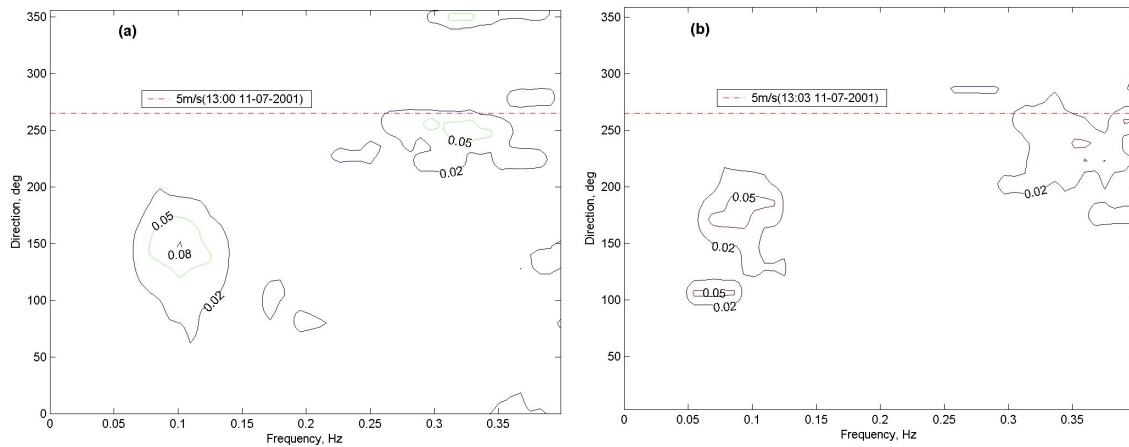


Figure 5. Measured directional wave spectra from (a) Mound Offshore at 13:00 GMT and (b) Oak Island at 14:03 GMT in November 7th, 2001 (surface wind is 5m/sec from 265° , shown as dash lines)

Examples shown in Figures 3, 4, and 5 suggest that the wave energy dissipation is smaller under the condition when the wave propagation is in the same direction as the wind direction than in the condition when the wave propagation is opposite to the wind direction. When the surface wind blows in the direction of the wave propagation, it tends to increase the horizontal water particle velocity under the wave trough and decrease the water particle velocity under the wave crest in the high frequency range. Under this condition, waves become less vulnerable to overturning and experience weaker breaking. On the other hand, when the wind and wave propagation are in opposite directions, the wind stress and wind-induced surface current tend to decrease the horizontal water particle velocity in the wave trough and increase the water particle velocity in the wave crest resulting in more wave over-turning and breaking.

In addition to the effect of different wind and wave directions, wave breaking will be strongly affected by the individual wave steepness, not the mean wave steepness. To illustrate the case, Figure 6 shows the wave spectral evolution at Mile 11 from 11:35 to 23:35 GMT in November 7th, 2001 under a mild offshore wind condition. In the time period of 11:35 to 17:35 GMT, the wind speed increased steadily from 5 to 7 m/sec and the wind direction changed gradually from 290° to 265° . In the time period of 17:35 to 23:35 GMT, the wind speed remained at 7 m/sec and the wind direction changed from 265° to 250° . In this example, the spectral evolution involves a bi-modal wave system (see Figure 4 for measured directional spectra) that consists of a swell, which appears as the lower frequency peak, and locally generated wind waves, associated with the higher frequency peak. It is evident that the mean wave steepness cannot represent the individual wave steepness in these spectra. Consequently, the wave breaking does not necessarily depend on the mean wave steepness. Because waves tend to break more as the individual wave steepness increases, it is essential to include the individual wave steepness in the wave breaking function formula.

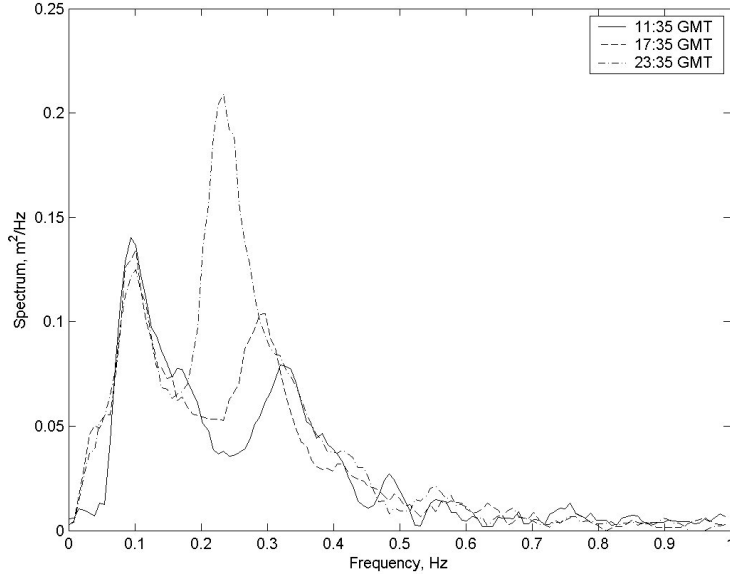


Figure 6. Wave spectral evolutions at Mile 11 from 11:35 to 23:35 in November 8th, 2001

New Wave Breaking Function

Based on the physical evidence revealed by the observed wave data, a new wave breaking function is formulated as

$$S_{wc}(\sigma, \theta) = -C_{ds} (ak)^n \frac{\sigma}{g} c_{wave}(\sigma, \theta) F_1(\bar{u}_{wind}, \bar{u}_{current}, \bar{c}_{wave}) F_2(h) E(\sigma, \theta) \quad (4)$$

$$\text{with } F_1(\bar{u}_{wind}, \bar{u}_{current}, \bar{c}_{wave}) = \left| \frac{\bar{c}_{wave}}{\bar{u}_{wind} + \bar{u}_{current} + \bar{c}_{wave}} \right|$$

$$F_2(h) = \begin{cases} \frac{1}{kh}, & \text{if } kh < 1; \\ 1, & \text{if } kh \geq 1. \end{cases}$$

where C_{ds} and n are constants to be determined from the observational data. To avoid the numerical instability and consider the physical constraint of energy loss during wave breaking, the function F_1 is set to equal to 2 if its computed value is greater than 2. A least square method is used to estimate C_{ds} and n from the following two steps:

$$\text{Step 1: Compute } \Delta = \sum_{i=1}^N (S_{data} - S_{wc})_i^2, \quad (5)$$

where S_{data} is the energy loss by wave breaking as observed in the data, and subscript i is the index of frequency and direction bands.

$$\text{Step 2: Solve } \frac{\partial \Delta}{\partial C_{ds}} = 0, \text{ and } \frac{\partial \Delta}{\partial n} = 0. \quad (6)$$

By using the data collected at Mound Offshore and Mile 11 in intermediate depth water, excluding the wind input energy into waves and energy loss from bottom friction, the best fit solutions are $C_{ds} = 0.03$ and $n = 1.5$ from Equations (5) and (6). In the estimation of C_{ds} and n , the surface current speed is assumed to be equal to 5% of the wind speed and the current direction is the same as the wind direction.

Figure 7, as an example using Equation (4), shows the deformation of a Person-Moskowitz spectrum, with an initial significant height (four times the square root of the total spectral energy) of 1.2 m in depth of 18 m, for the first 5 hours under the calm wind and pure wave breaking condition. It is seen that the energy dissipation under wave breaking is faster in the beginning and getting slower toward the end of the 5-hr simulation. The significant height is 0.4 m at the end of the 5-hr simulation. Figure 8 shows the similar simulation for wave breaking under a mild wind (wind speed equal to 5 m/sec) blowing in the same direction as the mean wave propagation. The wind input function is according to the formula developed by authors (Lin and Lin, 2004) in a separate paper. Figure 9 shows the similar simulation with the wind (wind speed equal to 5 m/sec) blowing in the opposite direction of the mean wave propagation. As a final example, Figure 10 shows the similar simulation with the wind (wind speed is 5 m/sec) blowing perpendicular to the mean wave propagation. For examples shown in Figures 8 to 10, the nonlinear wave-wave interaction is not simulated. In the real case, it is expected that the wave energy transfer from higher to lower frequencies will occur under wave-wave interactions.

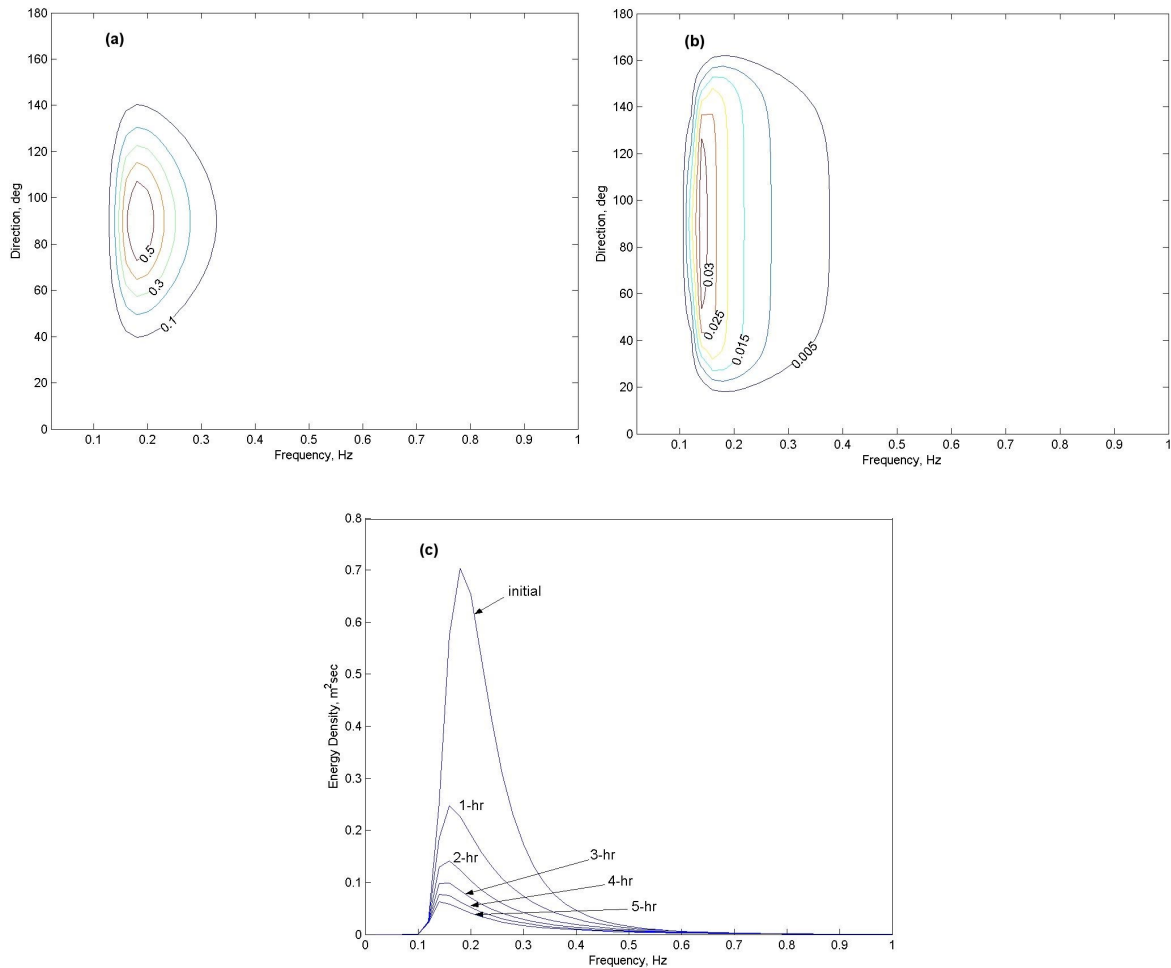


Figure 7. Spectral energy dissipation under wave breaking under the calm wind condition: (a) Initial spectrum, (b) spectrum after 5-hr simulation, (c) wave frequency spectral evolution during 5-hr simulation

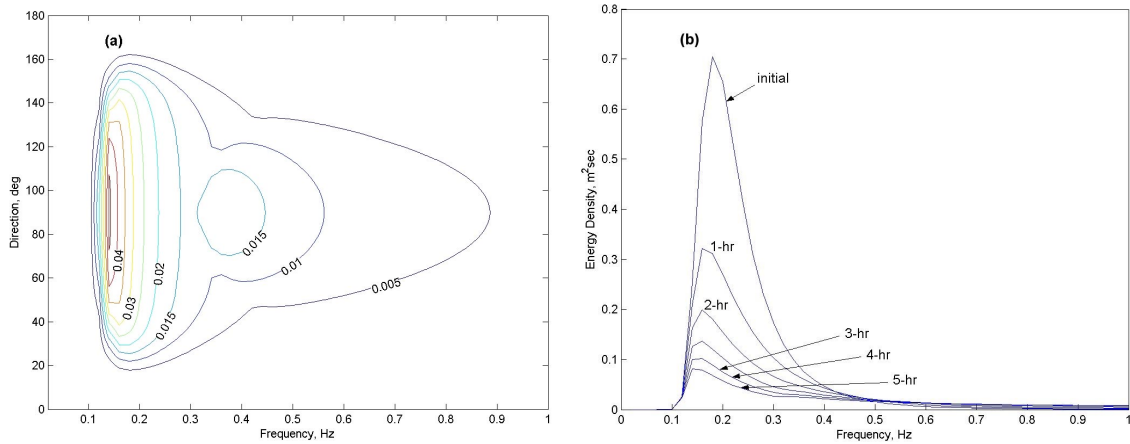


Figure 8. Spectral energy dissipation under wave breaking for a mild wind (wind speed is 5 m/sec) blowing in the same direction as wave propagation: (a) spectrum after 5-hr simulation, (b) wave frequency spectral evolution during 5-hr simulation

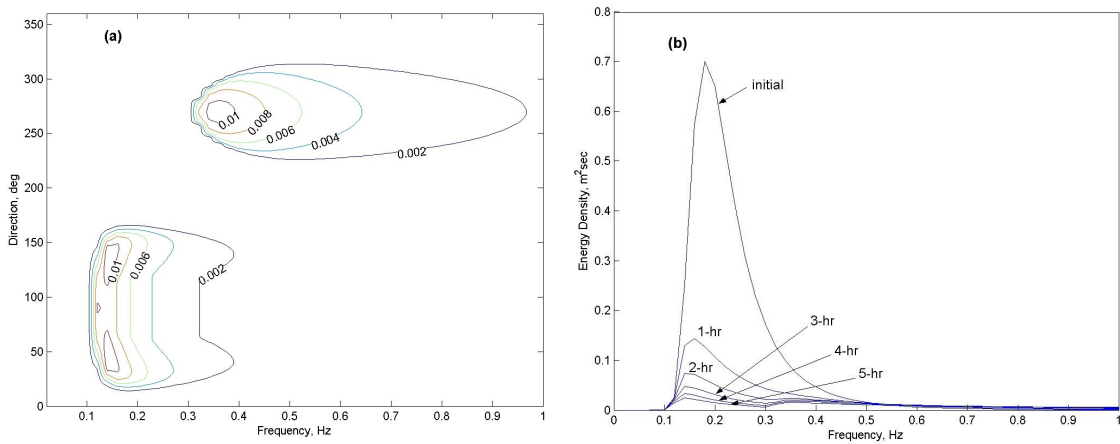


Figure 9. Spectral energy dissipation under wave breaking for a mild wind (wind speed is 5 m/sec) blowing in the opposite direction of the mean wave propagation: (a) spectrum after 5-hr simulation, (b) wave frequency spectral evolution during 5-hr simulation

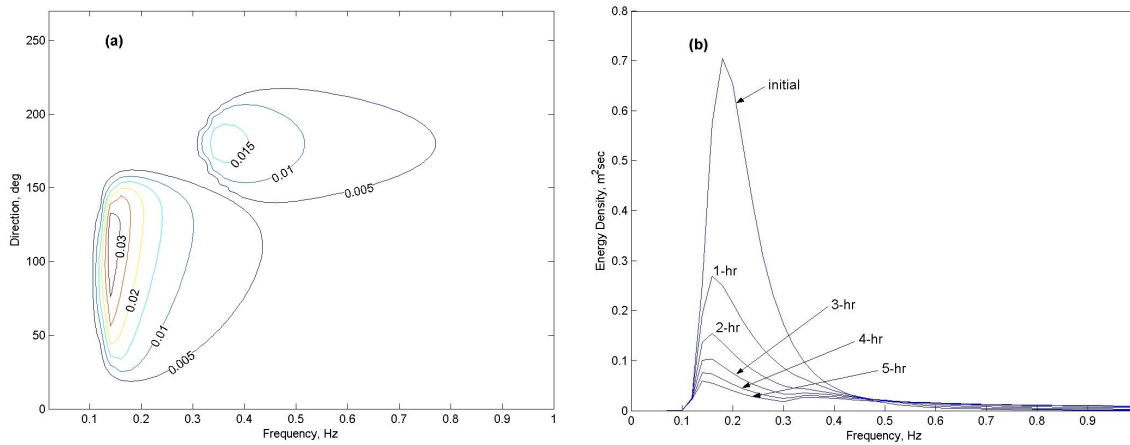


Figure 10. Spectral energy dissipation under wave breaking for a mild wind (wind speed is 5 m/sec) blowing perpendicular to the mean wave propagation: (a) spectrum after 5-hr simulation, (b) wave frequency spectral evolution during 5-hr simulation

4. SUMMARY

The new wave breaking function in the New Coastal wave Model (Lin and Huang, 1996a and Lin and Perrie, 1997a and b, 1999) was formulated to include individual wave steepness and wind effects of individual waves. This wave breaking function can predict the wave energy dissipation under the condition that the pure wind sea encounters a swell (Holthuijsen and Booij, 2000) as is often observed in the ocean. This function is intended to improve previous wave breaking formulae that are dependent on the mean wave steepness and mean phase velocity.

The new wave breaking function formula considers interactions among wind, current, and waves. It is well observed in the field that the ocean wave breaking is more severe in the condition when the wind and wave propagation are in opposite directions than the condition when the wind and wave propagation are in the same direction. This is because the surface current generated by the wind can increase the water particle velocity under the wave trough and decrease the water particle velocity in the crest when the wind and wave propagation are in the same direction. As a consequence, waves have less overturning and weaker breaking. However, when the wind and wave propagation are in the opposite direction, the wind will reduce the water particles moving speed and the wind-induced current can further decrease the water particle velocity in the wave trough resulting in more wave overturning and breaking. This physics is essential for the inclusion of the wind effect in the wave breaking sink function.

The new wave breaking formula includes the water depth limitation from a normalized water depth, kh . In the shallow water range, $kh < 1$, the longer wave can interact more with the bottom and break easier. Wave breaking due to the depth limitation is an important effect in the shallow water. It is well known that treating $2a_{wave}/h = 0.73$ as a constant does not always agree with the field data. In the application of spectral wave models, using a normalized water depth parameter, kh , in the wave breaking function should be more universal.

In the new wave breaking function, the proportional constant $C_{ds} = 0.03$ and power for wave steepness $n = 1.5$ were estimated based on very limited data. The wind input energy to waves is estimated in the calculation process. To more accurately estimate the wave breaking sink function, one must also couple the nonlinear wave-wave interaction term (Lin and Perrie, 1997a, 1999).

Acknowledgements

The authors would like to thank Mr. Michael Davis for providing many useful comments and suggestions to this study. We also thank Dr. John Barkyoub for supporting the numerical modeling project under the Naval Research Office In Laboratory Independent Research Program. Finally, we would like to thank Mr. Carl Miller for providing the field experiment data sets and Mr. Cliff Baron assisting in the management of the data. The U.S. Army Corps of Engineers (USACE) South Atlantic Division's Wilmington District maintains the Coastal Monitoring Program. Permission to publish this paper was granted by the Chief, USACE.

References

- Donelan, M. A. 1987. The Effect of Swell on the Growth of Wind Waves. Johns Hopkins APL Tech. Digest 8, 18-23.
- Eldeberky, Y. and Battjes, J.A. 1995. Parameterization of Triad Interactions in Wave Energy Models, Proc. Coastal Dynamics Conf. '95, Gdansk, Poland, 140-148.
- Hasselmann, K., Barnett, T.P., Bouws, E., Carlson, H., Cartwright, D.E., Enke, K., Ewing, J.A., Gienapp, H., Hasselmann, D.E., Krusemann, P., Meerburg, A., Muller, P., Olbers, D.J., Richter, K., Sell, W. and Walden, H., 1973. Measurements of Wind-Wave Growth and Swell Decay during the Joint North Sea Wave Project (JONSWAP), *Dtsch. Hydrogr. Z. Suppl.*, 12, A8.

- Hasselmann, K., 1974. On the Spectral Dissipation of Ocean Waves due to Whitecapping, *Bound. Layer Meteor.*, 6, 1-2, 107-127.
- Holthuijsen, L. H. and Booij, N. 2000. Oceanic and Near-Shore Whitecapping Effects in SWAN. The 6th International Workshop On Wave Hindcasting and Forecasting, Monterey, California. 362-368.
- Komen, G.J., Cavaleri, L., Donelan, M., Hasselmann, K., Hasselmann, S., and Janssen, P.A.E.M., 1994. Dynamics and Modeling of Ocean Waves. Cambridge University Press.
- Lin, R.-Q. and Huang, N.E. 1996a. The Goddard Wave Model, Part I. The Numerics, *J. Phys. Oceanogr.*, 26, 833-847.
- Lin, R.-Q. and Huang, N.E. 1996b. The Goddard Wave Model, Part II. Kinematics., *J. Phys. Oceanogr.*, 26, 848-862.
- Lin, R.-Q. and Lin, L. 2004. Wave Input Function. 8th International Workshop on Wave Hindcasting and Forecasting, North Shore, Oahu, Hawaii (Accepted).
- Lin, R.-Q. and Perrie, W. 1997a. A New Coast Wave Model Part III. Nonlinear Wave-Wave Interactions, *J. Phys. Oceanogr.*, 27, 1813-1826.
- Lin, R.-Q. and Perrie, W. 1997b. A New Coastal Wave Model Part V. Five-Wave Interactions, *J. Phys. Oceanogr.*, 28, 2169-2186.
- Lin, R.-Q. and Perrie, W. 1999. Wave-Wave Interactions in Finite Water Depth (A New Coastal Wave Model, Part IV), *J. Geophys. Res.*, 104, No. C5, 11193-11213.
- Longuet-Higgins, M. S. and Fox, M. J. H. 1977. Theory of the Almost-Highest Wave: The Inner Solution. *J. Fluid Mech.* 80, 721-741.
- Longuet-Higgins, M. S. and Fox, M. J. H. 1978. Theory of the Almost-Highest Wave. II. Matching and Analytic Extension, *J. Fluid Mech.* 85, 769-786.
- Michell, J. H. 1893. On the Highest Gravity Waves on Deep Water. *Phil. Mag.* 5, 36, 430.
- Phillips, O.M., and Banner, M.L. 1974. Wave Breaking in the Presence of Wind Drift and Swell. *J. Fluid Mech.* 66, part 4, 625-640.
- WAMDI group, 1988. The WAM Model-a Third Generation Ocean Wave Prediction Model, *J. Phys. Oceanogr.*, 18, 1775-1810.